Enhancement of Thermal Energy Transport Across Graphene/Graphite and Polymer Interfaces: A Molecular Dynamics Study

Tengfei Luo and John R. Lloyd**

Understanding thermal energy transport in polymeric nanocomposite materials is important to the engineering of polymer composites with better engineered heat transfer properties. Interfacial thermal resistance between the filling particles and the polymer matrices is a major bottleneck for the thermal conductivity improvement of polymer composite materials. Here, thermal energy transport in graphene/graphite-polymer (paraffin wax-$C_{30}H_{62}$) composite systems are systematically studied using molecular dynamics simulations. The influences of graphene size, interfacial bonding strength, and polymer density on the interfacial thermal transport are studied. According to the simulation results, approaches to improve interfacial thermal transport are proposed. Spectral analysis is performed to explore the mechanism of thermal transport. It is found that thermal energy transport across graphene/graphite-polymer interfaces can be enhanced by increasing the polymer density and graphene size or forming covalent bonds between the graphite edges and polymer molecules. The results offer valuable guidance on improving thermal transport properties of polymeric nanocomposite.

1. Introduction

Polymeric nanocomposite materials have been manufactured to enhance the mechanical, electrical, and thermal properties of pure polymers.[1–5] These nanocomposites have potential applications such as in aerospace,[6] automotive,[7] electronics,[8–10] energy systems,[11,12] etc. Among the various polymeric composites of current engineering interest, carbon nanotube (CNT) polymer nanocomposites have received significant attention[13–17] due to their exceptional mechanical, electrical, and thermal properties.[18–20] Graphene-based composite materials have become increasingly popular because graphene has similar thermal conductivity (≈3000 W mK^{-1}), mechanical stiffness (1060 GPa)[21] and electronic transport properties[22–25] as CNTs. Graphite, which is made of multiple layers of graphene, also have very high thermal conductivity in the in-plane direction (100–2000 W mK^{-1}).[26,27] Moreover, graphene and graphite are inexpensive (graphite is dollars per pound) compared to CNTs (hundreds of dollars per pound) and other nanoparticles.

Stankovich et al.[28] presented a general approach for the preparation of graphene-polymer composites via complete exfoliation of graphite, and extraordinary properties have been discovered with functionalized graphene-polymer nanocomposites.[29] Pure polymers usually have very low thermal conductivities (≈0.1–0.5 W mK^{-1}). Compositing thermally conductive graphene/graphite with thermally insulating polymers is expected to improve the effective thermal transport properties of the polymeric composite. The thermal conductivity enhancement in polymer-CNT composites, however, is limited to within one order of magnitude,[30] which is far from expectation. It has been found that interfacial thermal resistance between the filling particles and the polymer matrices present large barrier to the thermal transport in the composite materials.[31] While thermal transport in graphene, graphite and bulk polymers has been quite thoroughly investigated,[32–35] detailed investigation on thermal transport across interfaces between the graphene/graphite filling particles and the polymeric matrix is limited. This is of great importance in the improvement of thermally conductive graphene-polymer composite materials.

Konatham et al.[36] found that the thermal interface conductance of graphene-liquid oil ranges from 25-270 MW m^{-2} K^{-1} depending on the functionalization of the graphene edge. Using Nan's model,[37] Hu et al.[38] derived an effective interfacial thermal conductance of 30 MW m^{-2} K^{-1} between graphene and phenolic resin based on their molecular dynamics (MD) results. However, thermal conductance is found to be much lower (1–3 MW m^{-2} K^{-1})[39] at the CNT-polymer interface. Detailed thermal energy transport across these small scale interfaces is difficult to study through physical experiments, but MD simulations provide the possibility for a closer observation of the details of the interfacial transport phenomena.

Here, thermal conductances of graphene/graphite-polymer interfaces are calculated using non-equilibrium MD (NEMD). Analysis is carried out in the frequency domain to explore the

Prof. T. Luo
Aerospace and Mechanical Engineering
University of Notre Dame
Notre Dame, IN 46556, USA
E-mail: tluo@nd.edu
Prof. J. R. Lloyd
Mechanical and Aerospace Engineering
Naval Postgraduate School
Monterey, CA 93943, USA
E-mail: jrlloyd@nps.edu

DOI: 10.1002/adfm.201103048

Table 1. L-J potential parameters for different atom species (po: polymer; gr: graphene/graphite).

Atom type	Energy constant ε [eV]	Distance constant σ [Å]
H	0.000867	2.995
C_{po} (carbon in polymer)	0.002342	4.010
C_{gr} (carbon in graphene/graphite)	0.002390	3.412

mechanism of energy transport. According to the simulation results, approaches that can enhance interfacial thermal energy transport are discussed.

2. Methods and Simulations

In this study, the adaptive intermolecular reactive empirical bond order (AIREBO) potential,[40] which has been widely used in simulations of carbon systems and their thermal energy transport,[41] is used to model graphene and graphite. The condensed-phase optimized molecular potentials for atomistic simulation studies (COMPASS)[42] is used to model the polymer molecules. The COMPASS potential has been employed to study thermal energy transport in polymeric materials, and the calculated thermal conductivities are found to agree well with experiments.[43,44] The interactions between the graphene/graphite and polymers are mainly van der Waals interactions, which are modeled by Lenard–Jones (L-J) potentials. Lorentz–Berthelot mixing rules (ε_{ij} = sqrt($\varepsilon_i\varepsilon_j$); σ_{ij} = $(\sigma_i + \sigma_j)/2$, where ε and σ are the energy and distance constants, respectively. The subscripts i, j refer to different atom species.) are used to obtain the L-J parameters across different species of atoms. The L-J parameters for graphene/graphite atoms are from ref. [45] The L-J parameters of different atoms used in this study are included in **Table 1**. A L-J force cutoff of 10 Å is used.

The polymer simulated in this study is pure paraffin wax ($C_{30}H_{62}$) which has been widely used as a phase change material.[46] The predicted density using the COMPASS potential at 298 K and 1 atm is 0.89 g cc^{-1}, which agrees very well with experimental data of 0.87–0.91 g cc^{-1}.[47] The amorphous polymers are constructed using the modified Markov process[48] with bond conformational probabilities chosen to account for both intramolecular and intermolecular non-bonded interactions. The amorphous paraffin wax is then heated and slowly cooled for several iterations to release any uneven stress inside the polymer. Due to the presence of light-weighted hydrogen atoms, a time step of 0.25 fs is used for all simulations. The velocity-verlet scheme is used to integrate the equation of motion.

To calculate the interfacial thermal conductance, the steady state nonequilibrium method is applied to a system that consists of two amorphous polymer blocks with graphene/graphite in-between (**Figure 1**). Periodic boundary conditions are applied in the x- and y-directions.

For each simulation, the system is first optimized in isothermal–isobaric (NPT) ensembles with periodic boundary conditions applied to all three spatial directions. After the optimized structure and cell size are determined, simulation

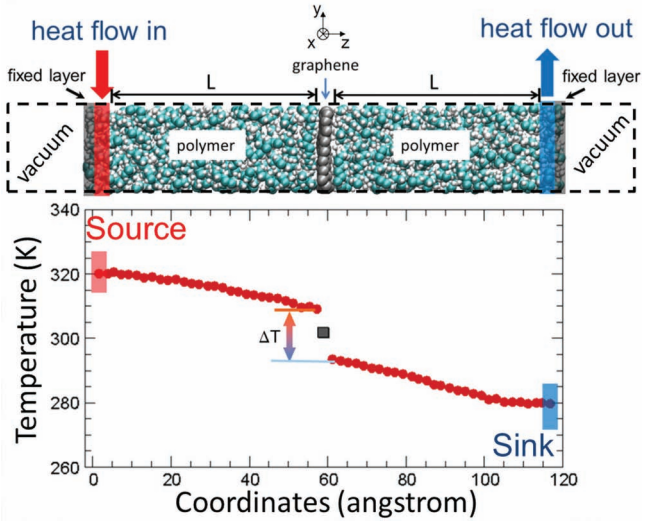

Figure 1. A system setup and an example steady state temperature profile of the polymer-graphene junction.

domain in the z-direction is made 20 Å larger than the equilibrium sample length to avoid interactions between the two ends. Very thin layers (3 Å) of polymer at the two ends of the sample are fixed to stabilize the free ends. Two 5 Å-thick layers next to these two fixed layer are thermostated using the Langevin scheme to maintain the heat sink and source region temperatures at different prescribed values so as to establish a temperature gradient across the junction. After steady state is reached, the interfacial thermal conductance (G) across the graphene/graphite and the polymer interface is calculated using $G = J/\Delta T$, where J is the heat flux and ΔT is the temperature difference across the interface as indicated in Figure 1. The final thermal conductance value is obtained by averaging data over 0.5 ns period in the steady state and the error bars are calculated using block averaging.

3. Results

3.1. Pure Polymer Validation

To test the COMPASS potential for thermal transport simulation, the thermal conductivity of pure amorphous paraffin wax ($C_{30}H_{62}$) was calculated using the non-equilibrium molecular dynamics (NEMD) and a value of 0.327 ± 0.017 W m^{-1} K^{-1} was determined. The AIREBO potential was also tested for the same purpose, and it yields a thermal conductivity of 0.332 ± 0.013 W m^{-1} K^{-1}. These values are in the range of experimental values of paraffin wax thermal conductivity (0.220 to 0.346 W m^{-1} K^{-1}).[49–51]

3.2. Influence of Graphene Size

The ideal graphene/graphite-polymer composite is when graphite is fully exfoliated into single graphene sheets. We

Table 2. Graphene-polymer interfacial conductance in systems with different polymer block lengths (L).

Polymer block length, L [Å]	Graphene-polymer interfacial conductance [MW m^{-2} K^{-1}]
35	61.14 ± 1.88
58	62.71 ± 4.10
82	61.04 ± 4.7

begin our study by considering thermal energy transport across the graphene-polymer interface using the NEMD method. The simulation geometry and an example steady state temperature profile have been presented in Figure 1. It is seen that there is an obvious temperature discontinuity at the graphene-polymer interface, suggesting a significant interfacial thermal resistance.

In MD, the simulation cell size is finite and can influence the calculated thermal transport properties since heat carriers with wavelengths longer than the cell sizes are not excited in the simulations, and phonon mean free paths are limited to the length of cell sizes.[44,52,53] This, however, provides an opportunity to study how the graphene and polymer block sizes influence the interfacial thermal transport.

For the polymer, the block length (L) was systematically varied from 35 Å, to 58 Å, and then to 82 Å. The interfacial thermal conductance of these systems was calculated. However, no obvious size dependence on the interfacial thermal conductance is observed (see **Table 2**).

One possible explanation for such observation is that in polymers, the major heat carriers are diffusive vibration modes, which have very short propagation length that are on the order of a few bond lengths.[34] The propagating vibration modes in amorphous materials, which are analogous to the propagating phonons in crystals, exhibit a very limited contribution to the total thermal conductivity at room or high temperatures.[35,44] The present results show that a block of size 35 Å is large enough to include all the important thermal transport modes in an amorphous polymer. However, the size effect can be significant in graphene,[32,54] where thermal conductivity is governed by propagating phonons, especially those long wavelength, long mean free path phonons.

To study the size effect on graphene, the cross sectional area was increased by replicating the smallest simulation cell ($X_o \times Y_o \times Z_o = 17.04 \times 19.68 \times 58.00$ Å^2, where X_o, Y_o, and Z_o are the dimensions of the smallest cell) in the y-direction. It is found that when the y-dimension is increased, the graphene-polymer interfacial thermal conductance increases from ≈61 MW m^{-2} K^{-1} until reaches a plateau of ≈71 MW m^{-2} K^{-1} (see **Figure 2**). When the graphene is elongated, the largest phonon wavelength ($l = Y$) allowed in the system is increased, where Y is the cell size in the y-direction (a schematic plot of $l = 4Y_o$ is shown as the inset of Figure 2).

The results in Figure 2 show that long wavelength phonons in graphene play important roles in graphene-polymer interfacial thermal transport. If it is assumed that the thermal conductance increment is solely due to the newly excited long wavelength phonons, the above results suggest that that phonons

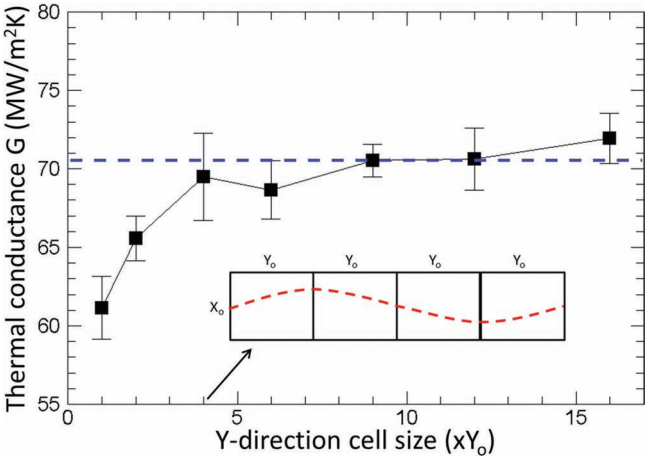

Figure 2. Interfacial thermal conductance as a function of simulation cell size in the y-direction. Inset: a schematic plot of $l = 4Y_o$.

with wavelength larger than 19.68 Å (Y_o) contribute about 15% of the total thermal conductance, and those with wavelength larger than 39.36 Å ($2Y_o$) have a contribution of about 7%. The results in Figure 2 also suggest that when the graphene flakes are shorter than about 78.72 Å ($4Y_o$), the polymer-graphene interfacial thermal conductance can be enhanced by increasing the length of the graphene flakes. However, such enhancement will be saturated when the graphene length is longer than about 78.72 Å ($4Y_o$), where all important modes contributing to the interfacial thermal transport are already excited.

Thermal energy, which is essentially the energy of atomic vibrations, can be characterized by the vibration power spectrum (VPS) in the frequency domain, which is calculated by taking the Fourier transform (FT) of the velocity autocorrelation functions (VAF) of atoms (see Equation 1).[55,56]

$$D(\omega) = \int_0^\tau \Gamma(t)\cos(\omega t)\mathrm{d}t \quad (1)$$

where ω is frequency, $D(\omega)$ is the VPS at frequency ω, and $\Gamma(t)$, which is given in Equation 2, is the VAF.

$$\Gamma(t) = \langle v(t)v(0)\rangle \quad (2)$$

Figure 3 shows the VPS of graphene carbon atoms and polymer carbon atoms. Since graphene is a highly anisotropic material, its VPS is decomposed into in-plane and out-of-plane spectra by taking the FT of VAF for velocity components in these corresponding directions separately.

It is seen that most of the overlap between polymer and graphene spectra lays at frequencies ranging from 2 to 16´THz, with the majority coming from the out-of-plane component of graphene vibration modes. This means that the out-of-plane motions of graphene atoms thermally couple better to polymer atoms. In another study, Hu et al.[57] also found that the coupling between graphene out-of-plane motion and polymer molecule motions at low frequencies serve as the most important channels for thermal transport across the interface. When more long wavelength phonons are excited due to the elongation of

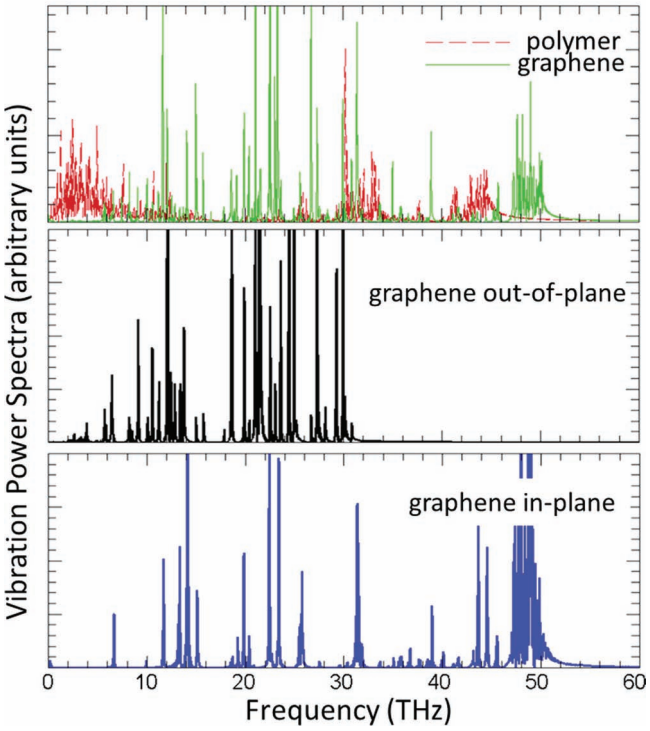

Figure 3. Vibration power spectra of polymer carbon atoms and graphene atoms with decomposition into out-of-plane and in-plane directions.

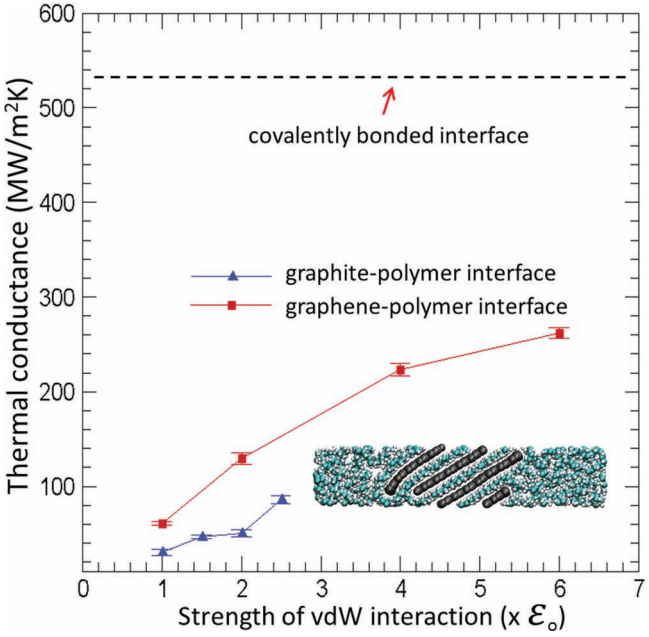

Figure 4. Thermal conductance as a function of interfacial van der Waals strength. Inset: graphite exfoliated when van der Waals strength is too strong.

the graphene flakes, there are more low frequency modes in graphene available to couple to polymer vibrations, and thus leading to larger interfacial thermal conductance. However, in the extremely low frequency region (< ≈1 THz), the polymer vibration density of state rapidly decreases, suggesting smaller population of vibration modes at these frequencies (see the top panel of Figure 3). As a result, when the graphene flakes are so long that the newly excited modes are with frequencies lower than ≈1 THz, there is no significant amount of low frequency modes in polymer to which these newly excited modes can couple. Thus a plateau is reached in thermal conductance as seen in Figure 2.

The calculated graphene-polymer interfacial thermal conductances, which are in the range from 61 to 71 MW m^{-2} K^{-1}, are on the same order of magnitude as previously reported graphene-oil interfacial conductances.[36] It should be noted that the calculated graphene-polymer interfacial conductance is more one order of magnitude larger than the CNT-polymer interfacial conductances (1–3 MW m^{-2} K^{-1}).[39] Besides the geometry difference between CNT and graphene, we also found that the transient lumped capacitance scheme used in ref. [39] yields lower thermal conductance than those obtained using the steady state NEMD scheme. The same observation was made by Hu et al.[38] in a recent study.

3.3. Interface Interaction Effect

From a microscopic point of view, thermal energy transport across an interface is accomplished through the interaction between the two groups of atoms at the two sides of the interface. In this section, the influence of the interfacial interaction strength on the thermal conductance is studied. To change the contact strength of the graphene-polymer system, in which the interfacial interactions are van der Waals forces, the energy constants of the L-J potential describing the interfacial van der Waals forces are increased by multiples of the original energy constant (i.e., $e = ne_o$, where e_o is the original energy constant and n is an integer number).

As shown in **Figure 4**, the graphene-polymer interfacial thermal conductance is greatly enhanced when the interfacial interaction is stronger. According to the fluctuation-dissipation theorem,[58] thermal conductance between two objects is proportional to the integrated autocorrelation of the net power (p) exchanged between them (Equation 3).

$$G \propto \int_0^\infty \langle p(0) \cdot p(t) \rangle \, \mathrm{d}t \tag{3}$$

The instantaneous net power exchanged between graphene and polymer is defined as

$$p = \sum_{\substack{i \in gr \\ j \in po}} F_{ij} \cdot v_j - \sum_{\substack{i \in gr \\ j \in po}} F_{ji} \cdot v_i \tag{4}$$

where F_{ij} is the force from atom j exerted on atom i, and v is atomic velocity. Stronger interactions at the interface lead to greater amplitude of net power and thus results in larger interfacial conductance. As a qualitative characterization of interfacial strength on thermal transport, we calculated autocorrelations of the net power (inset in **Figure 5**) across a graphene-polymer interface and integrated them over time (see Figure 5). Each curve is an average over results from 10 separate runs

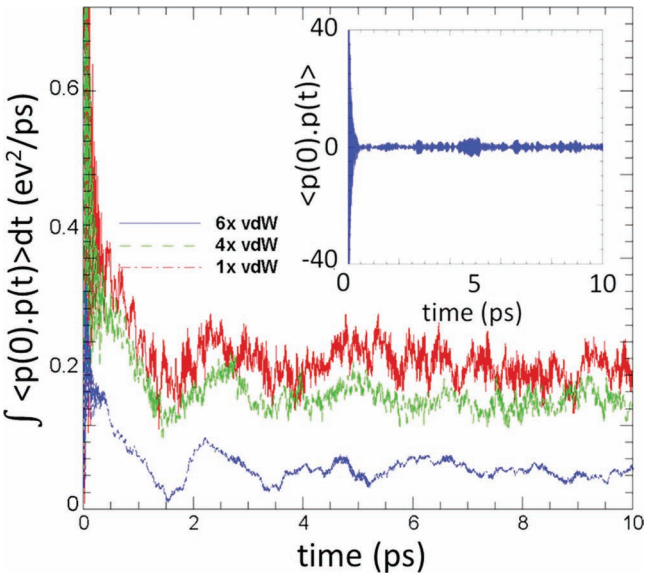

Figure 5. Integrated autocorrelation of net power exchanged at the interface as a function of interfacial van der Waals strength. Inset: a typical profile of a net power autocorrelation decay as a function of time.

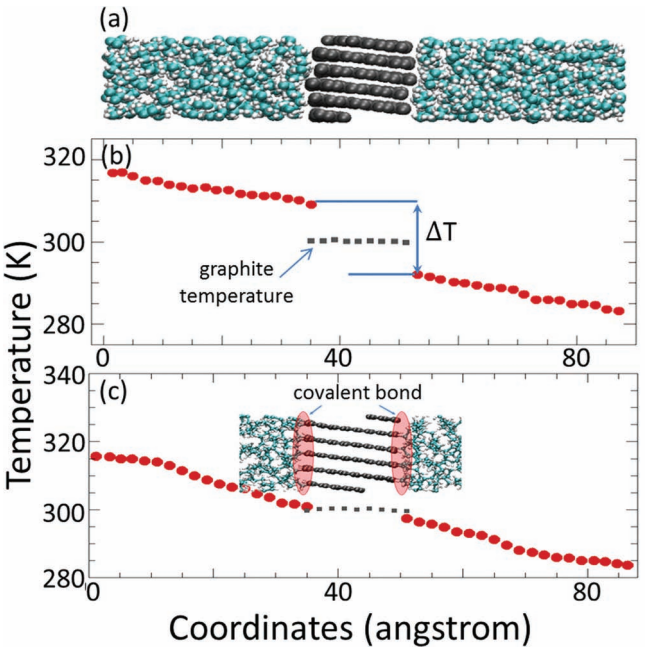

Figure 6. a) A simulation system setup of a graphite-polymer junction. b) A typical temperature profile of the graphite-polymer junction. c) Temperature profile of the covalently bonded graphite-polymer junction. Inset: graphite-polymer interface with covalent bonds.

with different initial conditions. It is seen in Figure 5 that the stronger the interfacial van der Waals strength is, the larger the integrated net power autocorrelation. Thus we see an increasing trend of thermal conductance as is reflected in Figure 4.

Such enhanced interfacial thermal transport due to interfacial strength increase cannot be easily realized practically. It is possible to enhance the van der Waals interaction by changing polymer species, but this will not significantly enhance the energy constant. A possible way of changing the interfacial strength is by altering the type of interaction from van der Waals forces to covalent bonds which are much stronger (e.g., in AIREBO potential, C–C covalent bond energy is about 5 eV[40] compared to C–C L-J energy constant of 0.00284 eV). It is difficult to form covalent bonds between the basal plane of the graphene and polymers since all bonds are saturated on the graphene surface. However, carbon atoms on the edge of the graphene have dangling bonds, thus leaving the possibility of forming covalent bonds with the environment.

To study such an effect, we construct a graphite-polymer junction as shown in **Figure 6**a. In practical applications for thermal transport, such geometries are actually preferred where heat flows parallel to the graphene/graphite basal plane that can take advantage of the ultrahigh in-plane thermal conductivities.

Interfacial thermal conductance between graphite and polymer is first calculated using the same potential model used in the graphene-polymer system (i.e., AIREBO for graphene, COMPASS for polymer, L-J for interaction between graphene and polymer). A nonequilibrium steady state temperature profile is presented in Figure 6b. There is almost no temperature gradient inside the graphite block, suggesting that the graphite has very high thermal conductivity in the in-plane direction. There are obvious temperature gradients in the polymer blocks and large temperature drops are found at the interface. The large temperature drops at the interface represent large thermal resistance, suggesting that the interfaces greatly limit the efficiency of thermal transport. We also found that if the graphene edge contacting polymer is zigzag, the conductance is 30.3 ± 3.3 MW m^{-2} K^{-1} and that of the armchair edge is 32.4 ± 3.8 MW m^{-2} K^{-1}, meaning that the orientation of the edge does not have significant impact on the interfacial thermal transport.

Similar to the graphene-polymer interface, a monotonic increase of the graphite-polymer interfacial thermal conductance is found when the interfacial van der Waals interaction is enhanced (see Figure 4). It is seen that the conductance of the graphite-polymer interface is lower than that of the graphene-polymer interface even though the van der Waals energy constants are the same. This is probably due to the fact that the graphite-polymer configuration has fewer carbon atoms per unit area at the interface (0.12 atoms Å^{-2}) than that of the graphene-polymer interface (0.38 atoms Å^{-2}), thus leading to weaker effective interfacial interaction. We also found that when van der Waals interaction is three times stronger than the original strength, polymer intercalates into the interstices of graphite layers and exfoliate the graphite into separate graphene sheets (see inset in Figure 4).

To capture possible formation of covalent bonds at the interface, the whole system, including polymer and graphite, is modeled using the AIREBO potential which is capable of simulating chemical reactions. At normal condition (i.e., room temperature, 1 atm), the thermal energy is found too low to overcome the reaction barrier to form covalent bonds, and thus the interfacial interaction is still connected by van der Waals forces. For such a van der Waals interface, the AIREBO yields a conductance of 35.9 ± 6.1 MW m^{-2} K^{-1}, which is comparable to the

results from simulations using the previous mixed potential model.

However, when the system is heated up to 800 K, covalent bonds start to form between polymer molecules and graphite edges. We further raise the system temperature to 1200 K where more covalent bonds are formed and then cool the system down to room temperature. There are 36 graphite-polymer bonds formed out of 80 carbon atoms with dangling bonds at the two edges of the graphite. The inset of Figure 6c highlights the covalent bonds at the interface. The steady state temperature profile in Figure 6c shows that the temperature jump across the interface is almost diminished. With these strong covalent bonds, interfacial thermal conductance is enhanced to ≈536 MW m^{-2} K^{-1}. This result suggests that forming strong covalent bonds between graphene/graphite filling particles with the polymer matrix eliminates the thermal transport bottleneck at the interface and can greatly improve the overall thermal conductivity of the polymeric composite. Similar observation was also made in a graphene-oil composite when the graphene flakes are functionalized with the oil molecules.[36]

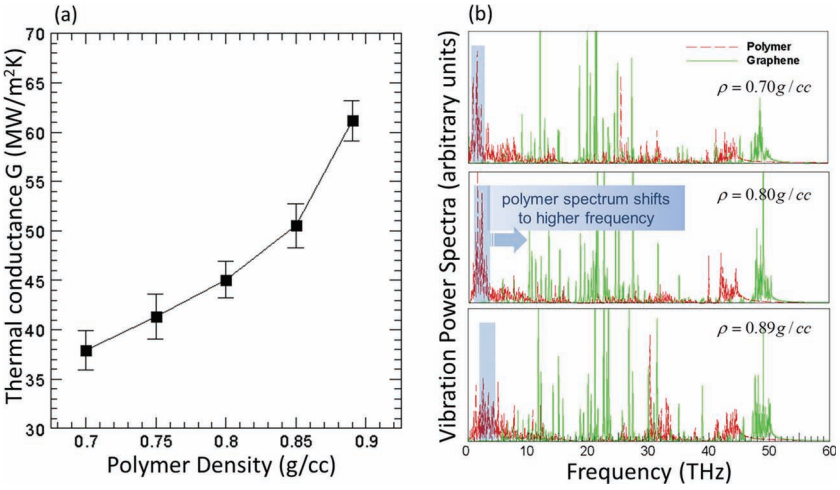

Figure 7. a) Graphene-polymer interfacial thermal conductance as a function of polymer density. b) Vibrational power spectra of graphene and polymer with different density.

3.4. Polymer Density Effect

The previous two sections show that the overlap between VPSs of materials at the two sides of the interface and the interfacial interaction strength can influence the thermal conductance. In this section, the influence of the polymer density on the interfacial thermal conductance is studied. This provides a third approach to enhance the interfacial thermal transport. In a polymer based composite material, the density of the polymer matrix can be easily changed by applying external pressure. We generate amorphous polymer at different densities separately and then optimize each structure using the procedure discussed in Section 2. The interfacial thermal conductance is then calculated. Through changing the polymer density, we found a monotonic increase of thermal conductance as the density increases from 0.7 g cc^{-1} to 0.89 g cc^{-1} (see **Figure 7**a).

When the amorphous structure is more compact, the interatomic distance is reduced. Such an effect can be visualized by analyzing the radial distribution function (RDF) of carbon atoms in polymer molecules at different polymer densities (see **Figure 8**).

It is seen that the first and the second peaks in the RDF, which correspond to atoms separated by one and two covalent bonds, have almost no change in magnitude. Because the covalent bond and angle strength are so strong, distances between atoms separated by one or two covalent bonds are difficult to alter even though the density is changed. However, the distribution function at larger separations (>3.5 Å) clearly shifts up when density is increased (inset of Figure 8a). Atoms separated by more than three bond distances mainly interact through weak van der Waals forces, thus making their interatomic distances easy to change through external pressure. Considering a simply relation between vibration frequency (w_o) and force constant (K), $w_o \approx \ddot{O}K$, the major source of the low frequency vibration modes are the weak van der Waals interactions which has force constants much smaller than bonded interactions. When the structure is compressed, the interatomic distance is shortened. The shorter interatomic distances (r) lead to effectively stronger van der Waals forces (F_{LJ}), which are modeled by LJ potentials as

$$F_{LJ} = -24\varepsilon\left[2\left(\frac{\sigma^{12}}{r^{13}}\right) - \left(\frac{\sigma^{6}}{r^{7}}\right)\right] \quad (5)$$

where ε is energy constant, σ is distance constant, and r is interatomic distance. Such increases in effective forces will in turn lead to higher vibration frequency ($w_o \approx$ sqrt(K)). Such an effect

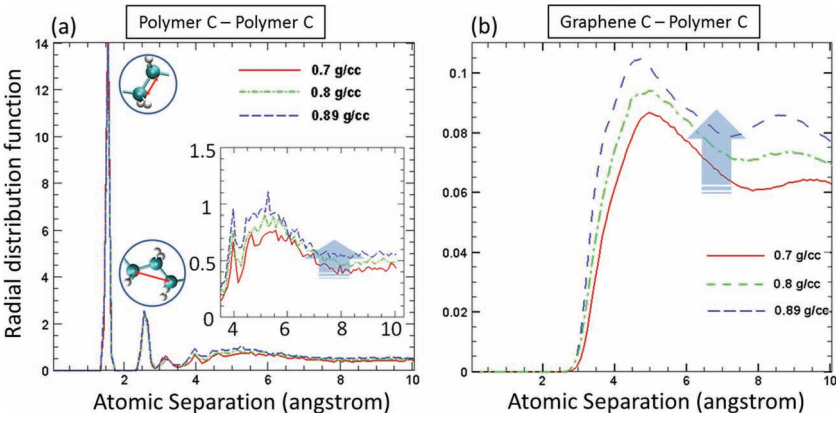

Figure 8. Radial distribution functions of a) carbon atoms in polymer molecules and b) carbon atoms in polymer with respect to carbon atoms in graphene.

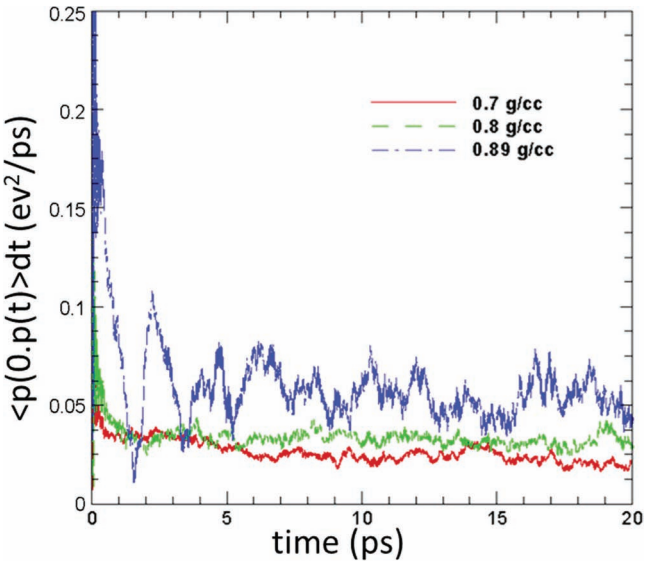

Figure 9. Integrated autocorrelation of net power exchanged at the interface as a function of polymer density.

is reflected in the VPS of polymer carbon atoms in Figure 7b. As can be seen in the figure, when polymer density increases, the low frequency spectra shift to the higher frequency side (see the peaks highlighted by the blue boxes), but no significant change of the graphene spectra is observed. As previously seen in Figure 3, the peaks of graphene spectra start at higher frequencies than those of polymer spectra. The shift of polymer spectra leads to greater overlap between the spectra of polymer and graphene whose significant vibration power starts from the frequency of 2 THz (see Figure 3). The greater spectra overlap leads to stronger thermal coupling, which in turn enhances thermal energy transport across the interface.

Besides the vibration spectra change of polymer, the more compact structure also leads to more polymer atoms interacting with graphene within the same distance, which results in stronger effective interactions between graphene and polymer. This is illustrated by the increasing RDF of polymer carbon atoms with respect to graphene atoms as shown in Figure 8b. To characterize the change of interfacial interaction, we again calculated the integrated interfacial net power autocorrelation function at different densities (see **Figure 9**). An increasing trend of the integrated autocorrelation function is observed, which suggests more effective thermal transport across the interface when polymer has higher density.

4. Conclusion

In conclusion, we used steady-state NEMD to calculate interfacial thermal conductance of graphene/graphite-polymer systems. We found that long wavelength phonons in graphene play important roles in thermal transport across the graphene-polymer interfaces. The existence of the low frequency modes (2–16 THz), due to out-of-plane motions, enables strong coupling between graphene spectra and polymer spectra and thus facilitates interfacial thermal transport. Interfacial interaction strength also influences thermal transport. The stronger the interactions are, the larger the thermal conductance. Microscopically, this effect is demonstrated by the integrated autocorrelation function of the net power exchanged at the interface. Forming strong covalent bonds between graphene/graphite edges and polymer molecules provides a practical approach to achieve more efficient thermal transport across the interface. Polymer density change leads to a shift of power spectra of low vibration mode in polymer. Such a shift results in greater vibration coupling between polymer and graphene, which provides another knob to tune the interfacial conductance.

The calculated interfacial thermal conductance can be used in macroscopic models[59–61] and experiments[62] to predict and analyze thermal transport in graphene/graphite-polymer composites. The approaches (i.e., elongating graphene flakes, forming strong covalent bonds at the interface, and increasing polymer density) explored in this study to enhance interfacial thermal transport provide practical guidance to the thermal conductivity improvement of polymeric composite.

Acknowledgements

The authors gratefully acknowledge the support of NSF Grant Award ID 0522594 to enable this work to be performed. T.L. thanks Professor Junichiro Shiomi from University of Tokyo and Dr. Keivan Esfarjani from MIT for useful discussions. This research was supported in part by the Notre Dame Center for Research Computing and NSF through TeraGrid resources provided by SDSC Trestles under grant number TG-CTS100078.

Received: December 15, 2011
Published online: March 29, 2012

[1] S. Komarneni, *J. Mater. Chem.* **1992**, *2*, 1219.
[2] J. Jordan, K. I. Jacob, R. Tannenbaum, *Mater. Sci. Eng. A* **2005**, *393*, 1.
[3] P. Podsiadlo, Z. Tang, B. S. Shim, N. A. Kotov, *Nano Lett.* **2007**, *7*, 1224.
[4] C. Luo, X. Zuo, L. Wang, E. Wang, S. Song, J. Wang, J. Wang, C. Fan, Y. Cao, *Nano Lett.* **2008**, *8*, 4454.
[5] J. M. Lehn, J. H. Fendler, F. Meldrum, *Adv. Mater.* **2004**, *7*, 607.
[6] B. Njuguna, K. Pielichowski, *Adv. Eng. Mater.* **2003**, *5*, 769.
[7] L. A. Goettler, K. Y. Lee, H. Thakkar, *Polym. Rev.* **2007**, *47*, 291.
[8] D. D. L. Chung, *J. Mater. Sci.* **2004**, *39*, 2645.
[9] J. Sung, Y. S. Choi, S. J. Kang, S. H. Cho, T. W. Lee, C. Park, *Nano Lett.* **2011**, *11*, 966.
[10] M. A. Priolo, D. Gamboa, K. M. Holder, J. C. Grunlan, *Nano Lett.* **2010**, *10*, 4970.
[11] C. Meng, C. Liu, L. Chen, C. Hu, S. Fan, *Nano Lett.* **2010**, *10*, 4025.
[12] G. Gustafsson, Y. Cao, G. M. Treacy, F. Klavetter, N. Colaneri, A. Heeger, *Nature* **1992**, *357*, 477.
[13] E. T. Thostenson, Z. Ren, T. W. Chou, *Compos. Sci. Tech.* **2001**, *61*, 1899.
[14] X. Dang, H. Yi, M. Han, J. Qi, D. S. Yun, R. Ladewski, M. S. Strano, P. T. Hammond, A. M. Belcher, *Nat. Nanotechnol.* **2011**, *6*, 377.
[15] F. M. Toma, A. Sartorel, M. Iurlo, M. Carraro, P. Parisse, C. Maccato, S. Rapino, B. R. Gonzalez, H. Amenitsch, T. Da Ros, L. Casalis, A. Goldoni, M. Marcaccio, G. Scorrano, G. Scoles, F. Paolucci, M. Prato, M. Bonchio, *Nat. Chem.* **2010**, *2*, 826.

[16] M. J. Biercuk, M. C. Llaguno, M. Radosavljevic, J. K. Hyun, A. T. Johnson, J. E. Fischer, *Appl. Phys. Lett.* **2002**, *80*, 2767.
[17] S. U. S. Choi, Z. G. Zhang, W. Yu, F. E. Lockwood, E. A. Grulke, *Appl. Phys. Lett.* **2001**, *79*, 2252.
[18] M. S. Dresselhaus, G. Dresselhaus, P. Avouris, *Carbon Nanotubes: Synthesis, Structure, Properties, Applications*, Springer, New York **2000**.
[19] J. Y. Huang, S. Chen, Z. Q. Wang, K. Kempa, Y. M. Wang, S. H. Jo, G. Chen, M. S. Dresselhaus, Z. F. Ren, *Nature* **2006**, *439*, 281.
[20] S. Berber, Y. K. Kwon, D. Tomanek, *Phys. Rev. Lett.* **2000**, *84*, 4613.
[21] S. Stankovich, D. A. Dikin, G. H. B. Dommett, K. M. Kohlhaas, E. J. Zimney, E. A. Stach, R. D. Piner, S. T. Nguyen, R. S. Ruoff, *Nature* **2006**, *442*, 282.
[22] K. S. Novoselov, A. K. Geim, S. V. Morozov, D. Jiang, M. I. Katsnelson, I. V. Grigorieva, S. V. Dubonos, A. A. Firsov, *Nature* **2005**, *438*, 197.
[23] K. S. Novoselov, A. K. Geim, S. V. Morozov, D. Jiang, Y. Zhang, S. V. Dubonos, I. V. Grigorieva, A. A. Firsov, *Science* **2004**, *306*, 666.
[24] Y. Zhang, Y. W. Tan, H. L. Stormer, P. Kim, *Nature* **2005**, *438*, 201.
[25] Y. Zhang, J. P. Small, M. E. S. Amori, P. Kim, *Phys. Rev. Lett.* **2005**, *94*, 176803.
[26] M. Smalc, G. Shives, G. Chen, S. Guggari, J. Norley, *Proc. ASME InterPACK*, San Francisco, CA, July 17–22, **2005**, paper no. 2005–73073.
[27] K. Sun, M. A. Stroscio, M. Dutta, *Superlattices Microstruct.* **2009**, *45*, 60.
[28] S. Stankovich, R. D. Piner, X. Chen, N. Wu, S. T. Nguyen, R. S. Ruoff, *J. Mater. Chem.* **2006**, *16*, 155.
[29] T. Ramanathan, A. A. Abdala, S. Stankovich, D. A. Dikin, M. Herrera-Alonso, R. D. Piner, D. H. Adamson, H. C. Schniepp, X. Chen, R. S. Ruoff, S. T. Nguyen, I. A. Aksay, R. K. Prud'Homme, L. C. Brinson, *Nat. Nanotechnol.* **2008**, *3*, 327.
[30] M. Moniruzzaman, K. I. Winey, *Macromolecules* **2006**, *39*, 5194.
[31] S. T. Huxtable, D. G. Cahill, S. Shenogin, L. P. Xue, R. Ozisik, P. Barone, M. Usrey, M. S. Strano, G. Siddons, M. Shim, P. Keblinski, *Nat. Mater.* **2003**, *2*, 731.
[32] J. H. Seol, I. Jo, A. L. Moore, L. Lindsay, Z. H. Aitken, M. T. Pettes, X. Li, Z. Yao, R. Huang, D. Broido, N. Mingo, R. S. Ruoff, L. Shi, *Science* **2010**, *328*, 213.
[33] P. G. Klemens, D. F. Pedraza, *Carbon* **1994**, *32*, 735.
[34] P. B. Allen, J. L. Feldman, *Phys. Rev. Lett.* **1989**, *62*, 645.
[35] P. B. Allen, J. L. Feldman, J. Fabian, F. Wooten, *Philos. Mag. Part B* **1999**, *79*, 1715.
[36] D. Konatham, A. Striolo, *Appl. Phys. Lett.* **2009**, *95*, 163105.
[37] C. W. Nan, R. Birringer, D. R. Clarke, H. Gleiter, *J. Appl. Phys.* **1997**, *81*, 6692.
[38] L. Hu, T. Desai, P. Keblinski, *J. Appl. Phys.* **2011**, *110*, 033517.
[39] C. F. Carlborg, J. Shiomi, S. Maruyama, *Phys. Rev. B* **2008**, *78*, 205406.
[40] S. J. Stuart, A. B. Tutein, J. A. Harrison, *J. Chem. Phys.* **2000**, *112*, 6472.
[41] J. Hu, X. Ruan, Y. P. Chen, *Nano Lett.* **2009**, *9*, 2730.
[42] H. Sun, *J. Phys. Chem. B* **1998**, *102*, 7338.
[43] J. Liu, R. Yang, *Phys. Rev. B* **2010**, *81*, 174122.
[44] T. Luo, K. Esfarjani, J. Shiomi, A. Henry, G. Chen, *J. Appl. Phys.* **2011**, *109*, 074321.
[45] L. A. Girifalco, M. Hodak, R. S. Lee, *Phys. Rev. B* **2000**, *62*, 13104.
[46] J. Xiang, L. T. Drzal, *Sol. Energy Mater. Sol. Cells* **2011**, *95*, 1811.
[47] R. C. West, *CRC Handbook of Chemistry and Physics*, 68th edition, CRC Press, Boca Raton, FL, **1987–1988**.
[48] M. P. Allen, D. J. Tildesley, *Computer Simulation of Liquids*, Oxford University Press, New York **1987**.
[49] Sari, A. Karaipekli, *Appl. Thermal Eng.* **2007**, *27*, 1271.
[50] H. Ettouney, H. El-Dessouky, A. Al-Ali, *J. Sol. Energy Eng.* **2005**, *127*, 357.
[51] G. A. Lane, *Int. J. Energy Res.* **1980**, *5*, 155.
[52] P. K. Schelling, S. R. Phillpot, P. Keblinski, *Phys. Rev. B* **2002**, *65*, 144306.
[53] D. P. Sellan, E. S. Landry, J. E. Turney, A. J. H. McGaughey, C. H. Amon, *Phys.Rev. B* **2010**, *81*, 214305.
[54] N. Mingo, K. Esfarjani, D. A. Broido, D. A. Stewart, *Phys. Rev. B* **2010**, *81*, 045408.
[55] T. Luo, J. R. Lloyd, *Int. J. Heat Mass Transfer* **2010**, *53*, 1.
[56] T. Luo, J. R. Lloyd, *J. Appl. Phys.* **2011**, *109*, 034301.
[57] L. Hu, T. Desai, P. Keblinski, *Phys. Rev. B* **2011**, *83*, 195423.
[58] G. Domingues, S. Volz, K. Joulain, J. J. Greffet, *Phys. Rev. Lett.* **2005**, *94*, 085901.
[59] K. Bui, B. P. Grady, D. V. Papavassiliou, *Chem. Phys. Lett.* **2011**, *508*, 248.
[60] K. Bui, H. M. Duong, A. Striolo, D. V. Papavassiliou, *J. Phys. Chem. C* **2011**, *115*, 3872.
[61] D. Konatham, K. Bui, D. V. Papavassiliou, A. Striolo, *Mol. Phys.* **2011**, *109*, 97.
[62] J. E. Peters, D. V. Papavassiliou, B. P. Grady, *Macromolecules* **2008**, *41*, 7274.